Journal of Ultrafine Grained and Nanostructured Materials
https://jufgnsm.ut.ac.ir
Vol. 50, No.2, December 2017, pp. 137-151
Print ISSN: 2423-6845 Online ISSN: 2423-6837
DOI: 10.22059/JUFGNSM.2017.02.09

Scattering Study of Conductive-Dielectric Nano/Micro-grained Single Crystals Based on Poly(ethylene glycol), Poly(3-hexyl thiophene) and Polyaniline

Samira Agbolaghi*[1] , Sahar Zenoozi[2], Saleheh Abbaspoor[2], Maryam Nazari[3]

[1] *Chemical Engineering Department, Faculty of Engineering, Azarbaijan Shahid Madani University, Tabriz, Iran.*

[2] *Institute of Polymeric Materials and Faculty of Polymer Engineering, Sahand University of Technology, Tabriz, Iran.*

[3] *Department of Chemistry, University of Calgary, Calgary, Canada.*

Recieved: 14 February 2017; Accepted: 16 October 2017

** Corresponding author email: chemeng96sa1987@yahoo.com*

ABSTRACT

Two types of rod-coil block copolymers including poly(3-hexylthiophene)-block-poly(ethylene glycol) (P3HT-b-PEG) and PEG-block-polyaniline (PANI) were synthesized using Grignard metathesis polymerization, Suzuki coupling, and interfacial polymerization. Afterward, two types of single crystals were grown by self-seeding methodology to investigate the coily and rod blocks in grafted brushes and ordered crystalline configurations. The conductive P3HT fibrillar single crystals covered by the dielectric coily PEG oligomers were grown from toluene, xylene, and anisole, and characterized by atomic force microscopy (AFM) and grazing wide angle X-ray scattering (GIWAXS). Longer P3HT backbones resulted in folding, whereas shorter ones had a high tendency towards backbone lamination. The effective factors on folding of long P3HT backbones in the single crystal structures were the solvent quality and crystallization temperature. Better solvents due to decelerating the growth condition led to a higher number of foldings. Via increasing the crystallization temperature, the system decreased the folding number to maintain its stability. Poorer solvents also reflected a higher stacking in hexyl side chain and π-π stacking directions. The dielectric lamellar PEG single crystals sandwiched between the PANI nanorods were grown from amyl acetate, and analyzed using the interface distribution function (IDF) of SAXS and AFM. The molecular weights of PANI and PEG blocks and crystallization temperature were focused while studying the grown single crystals.

Keywords: *P3HT; PEG; PANI; single crystal; self-seeding; GIWAXS; SAXS.*

How to cite this article:
Agbolaghi S, Zenoozi S, Abbaspoor S, Nazari M. Scattering study of conductive-dielectric nano/micro-grained single crystals based on poly(ethylene glycol), poly(3-hexyl thiophene) and polyaniline. J Ultrafine Grained Nanostruct Mater, 2017; 50(2):137-151.

1. Introduction

Semiconducting polymers particularly poly(3-hexylthiophene) (P3HT) have been widely studied in semiconductor devices like solar cells [1–11], field effect transistors [12–16], light emitting diodes [17], chemical sensors [18] and thin film transistors [19]. In conductive materials field, the large single rectangular crystals of regioregular octamer of 3-hexyl-thiophene $(3HT)_8$ [20,21], well-defined single crystalline nanowires of conjugated poly(*p*-phenylene ethynylene) derivatives [22], single P3HT nano-whiskers [23], one dimensional (1D) microwire P3HT single crystals [24,25] and self-organized two dimensional (2D) P3HT

supramolecules [26,27] were reported. The principle method for single crystal preparation was the self-seeding procedure [28–30]. Kim et al. [24] worked on one dimensional single crystalline P3HT microwires grown by the self-assembly process in dilute chloroform solution. In another work, the scrolled half-ring crystals were reported for P3HT-based materials [31]. The thermal and optical properties of P3HT homopolymers and block copolymers were also focused [32]. The P3HT and poly(3-octylthiophene) (P3OT) single crystals were also prepared via vapor annealing and solvent evaporation by Xiao et al. [33,34]. Rahimi et al. [20] demonstrated that the large single crystals can be grown from both short regioregular oligomers and long P3HT chains. They also reported that charge transport through the single crystal was anisotropic [21]. The P3HT single crystals absorbed light at higher wavelengths compared to spin cast films and thus a remarkable red shift occurred [35]. The crystalline whiskers [36], crystalline nanofibrils [37,38], and single crystalline 2D nanosheets [39] were also reported for P3HT.

In the family of π-conjugated polymers, polyaniline (PANI) has also unique properties such as diverse structures, good environmental stability, low cost and simple acid/base doping/dedoping chemistry [40,41]. The PANI is a promising material for a wide range of applications in different fields, for example, anticorrosion coatings [42], batteries [43], potentiometric sensors [44], membranes [45], antistatic coatings [46], electromagnetic shields [47], catalyst [47], high-rate supercapacitors [48,49] and fluorescent sensing for nucleic acid detection [50]. The novel patterned structures of nano/micro conductive-dielectric channels designed by single crystals were recently reported, in which the PANI nanorods were tethered onto a crystalline substrate as polymer brushes [51]. The fourth regime or extremely extended regime of polymer brushes was also innovated based on conductive PANI brush-covered single crystals [52]. From the perspective of characterization, the polymer single crystals were investigated using atomic force microscopy (AFM) [53–60], X-ray scattering [51,61], transmission electron microscopy (TEM) [34,62], field emission scanning electron microscopy (FESEM) [24], scanning electron microscopy (SEM) [34], and small angle neutron scattering (SANS) [63].

In the current work, two types of rod-coil block copolymers including P3HT-*b*-PEG and PEG-*b*-PANI were synthesized and used as building blocks of crystalline structures by self-seeding methodology. The P3HT-*b*-PEG block copolymers reflected the fibrillar crystals composed of stacked P3HT backbones, in which the PEG coily blocks were accumulated on the crystal surface. On the other side, the PEG-*b*-PANI copolymers led to the square PEG single crystals sandwiched between PANI nanorods grafted as polymer brushes. Indeed, we designed two distinct sorts of single crystals by a unique processing approach but various configurations to investigate the impact of material type on crystalline structure. In grown P3HT-*b*-PEG and PEG-*b*-PANI single crystals, the coily PEG blocks were in the roles of accumulated hairy brushes and a crystalline substrate, respectively. In addition, some other parameters such as molecular weight and solvent quality were considered while developing and studying the single crystals.

2. Experimental

2.1. Synthesis of P3HT based materials

Highly regioregular P3HTs (>99%) with different molecular weights (M_n^{P3HT}) and the polydispersity index (PDI) of 1.21–1.25 were synthesized using Grignard metathesis polymerization [64]. A dry 100 mL two-neck flask was flushed with N_2 and charged with 2,5-dibromo-3-hexylthiophene and dried THF (30 mL). A 1 M solution of methyl magnesium bromide (MeMgBr) in THF was added via a syringe, and refluxed for 2 h under an atmosphere of nitrogen. 1,3-bis(diphenylphosphino) propane nickel(II) chloride (Ni(dPPP)) in 8 mL anhydrous THF was added in one portion, and refluxing was continued for 100 min. The molar ratio of monomer/MeMgBr/Ni(dPPP) as a type for M_n^{P3HT} = 21000 g/mol was 1/1/0.02. Subsequently, the reaction mixture was concentrated to 10 mL and was dropped in methanol under vigorous stirring. The precipitate was collected by filtration and washed with methanol. The crude polymer was then exhaustively Soxhlet-extracted with methanol and hexane to remove residual catalysts and short polymer chains.

The P3HT-*b*-PEG_{750} rod-coil block copolymers were synthesized with Suzuki coupling [65]. The PEG, 4-(4,4,5,5-tetramethyl-1,3,2-dioxaborolan-2-yl) benzoic acid (DBA), and anhydrous THF (60 mL) were added to a two-necked flask under nitrogen. Then, N,N-dicyclohexylcarbodiimide (DCC) and N,N-dimethylaminopyridine (DMAP) were added and the mixture was stirred for 24 h at room temperature. The molar ratio of PEG/

DBA/DCC/DMAP was 0.33/1.16/1/1 [65]. The precipitation was filtered off, and the mixture was then poured into diethyl ether. The precipitation was collected by filtration and washed with diethyl ether. The product was accomplished by column chromatography on silica with dichloromethane:methanol (10:1) to acquire the polymer. To a two-necked flask equipped with a stopcock were added P3HT-Br, PEG-BE, palladium-tetrakis(triphenylphosphine) ($Pd(PPh_3)_4$), and dried toluene (13 mL) under nitrogen. After that 3 M K_2CO_3 aq. (3 mL) was added and the mixture was stirred at 100 °C for 24 h. The solution was concentrated and poured into methanol to give the polymer. The polymer was extracted with methanol and acetone.

2.2. Synthesis of PANI based materials

The PEG-*b*-PANI diblock and PANI-*b*-PEG-*b*-PANI triblock copolymers were synthesized by an interfacial polymerization [55]. To this end, the three macroinitiators (amine-terminated polyethylene glycol benzoate (ATPEGB)), i.e., $ATPEGB_{5000}$, $ATPEGB_{6000}$ and $ATPEGB_{35000}$ were first synthesized. The PEG and 4-amino benzoic acid (equivalent moles) and xylene (100 mL for PEG 5000 and 6000, 120 mL for PEG 35000) were taken into a two-necked reaction flask fitted with stirrer and a Dean and stark trap. The catalytic amount of *p*-toluene sulfonic acid (PTSA) was added to the mixture. The mixture was heated to reflux temperature (140 °C). The water of reaction was removed as an azeotrope until the reaction was completed during refluxing at 140 °C for 5 h. The solvent then was removed off under reduced pressure and the solid product was dissolved in chloroform. The unreacted 4-amino benzoic acid was then filtered and the solvent of obtained solution was evaporated. The final solid product was dried under vacuum for 48 h.

Subsequently, ammonium peroxydisulfate (APS) and potassium hydrogen biiodate (PHD) was dissolved in sufficient amount of 1 M sulfuric acid solution in a 400-mL beaker. This was done gently and with minimal agitation along the sides of beaker. The aniline/ATPEGB/chloroform solution formed lower organic layer and ammonium peroxydisulfate/potassium hydrogen biiodate solution formed upper aqueous layer. After a short induction period from 1 min (using ammonium peroxydisulfate) to 15 min (using potassium hydrogen biiodate), green polyaniline appeared at the interface, migrating into the water phase, and finally filling entire water layer. An overnight reaction time was generally appropriate to complete the reaction. Then, the solid polymer consisting aniline homopolymers and block copolymers was filtered. The unreacted PEG from etherification step was soluble in chloroform and could not enter into the structure of copolymers. This precipitate was poured into methanol, the aniline homopolymer was insoluble in methanol, but PANI-*b*-PEG-*b*-PANI (or PEG-*b*-PANI) was soluble in this solvent. The mixture was stirred for 12 h and then filtered. The solid aniline homopolymer was removed off and the resulting dark brown solution was purified.

2.3. Single crystal growth

The P3HT-*b*-PEG single crystals were grown in toluene (here best solvent), xylene (as an intermediate solvent), and anisole (as a poor solvent) using the self-seeding method with the concentration of 0.01 wt%. The single crystals were grown at different seeding temperatures (T_s) and crystallization temperatures (T_c). To reach the homogeneous solutions, the prepared dispersions were heated for 30 min at 75 °C in toluene, at 85 °C in xylene, and at 95 °C in anisole. The samples were then kept at 0 °C overnight. The next step was seeding and was conducted for 3 min at respective T_s. Subsequently, the samples were kept at T_c for 3 days.

The self-seeding procedure was also utilized to grow the PEG single crystals covered by conductive PANI nanorods. Solution crystallization was carried out with a dilute concentration of 0.009 wt% in amyl acetate. The vials containing PEG-*b*-PANI diblock and PANI-*b*-PEG-*b*-PANI triblock copolymers were sealed and kept at dissolution temperature (T_d = 70 °C) for 30 minutes. The samples were then kept at primary crystallization of 0 °C for 5 h and the self-seeding temperature of T_s = 41 °C for 20 min. The vials were then transferred into an isothermal oil bath set at crystallization temperature and were maintained for 3 days to complete the single crystal growth process.

2.4. Characterization

The grazing incidence wide-angle X-ray scattering (GIWAXS) patterns were collected by a CMOS flat panel X-ray detector (C9728DK) and a CCD detector (MAR165, 165 mm in diameter, 1024 by 1024 pixels resolution). The layer spacings between crystallographic planes were calculated from $(100)_{OOP}$

and $(020)_{IP}$ Bragg peaks position for the edge-on (with the alkyl chain perpendicular to substrate) P3HT single crystals [66]. The normal SAXS analyses were conducted on Bruker-AXS Nanostar SAXS with a counts rate of 1000 s/sec/channel and spatial resolution of 400-500 μm. Furthermore, the dimensions of P3HT single crystals were monitored with an AFM Nanoscope III.

3. Results and discussion

3.1. Fibrillar P3HT single crystals covered with PEG coils

FT-IR and ^{1}HNMR spectra of synthesized $P3HT_{7000}$-Br are represented in Figs. 1(a) and (b), respectively. In FT-IR spectrum (Fig. 1(a)), the end C–Br bands were detected at 620 and 1240 cm^{-1}. The main chains peaked at 832, 1456, 1510 and 3054 cm^{-1} and the side chains were characterized based on 728, 1378, 2856, 2926 and 2955 cm^{-1} peaks. In ^{1}HNMR spectrum (Fig. 1(b)), the head-to-tail/head-to-tail (HT-HT) peak appeared at 6.98 ppm. The molecular weight of P3HT block was determined using the intensities at 2.6 and 2.8 ppm.

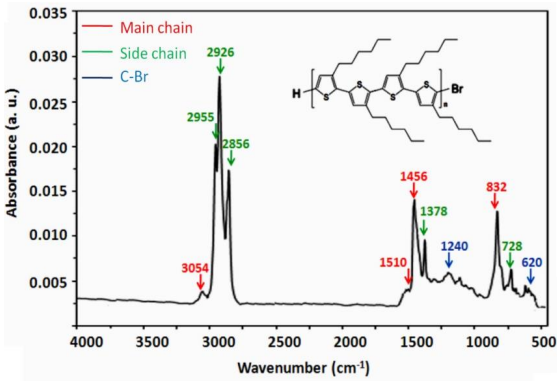

(a)

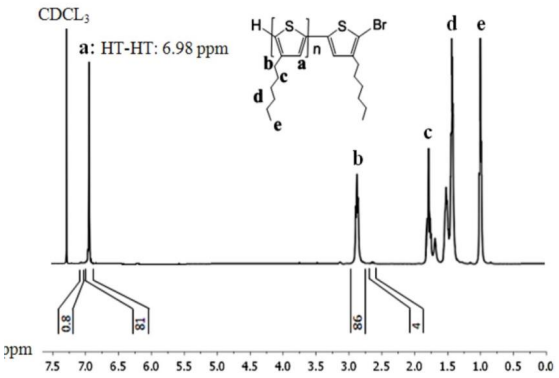

(b)

Fig. 1- FT-IR (a) and 1HNMR (b) spectra of synthesized P3HT7000-Br.

Figs. 2(a-c) represent ^{1}HNMR spectra of $P3HT_{48800}$-Br, $P3HT_{21000}$-Br, and $P3HT_{7150}$-Br. The HT-HT configurations appeared at 6.98 ppm. The other configurations including tail-to-tail/head-to-tail (TT-HT), head-to-head/head-to-tail (HH-HT), and tail-to-tail/head-to-head (TT-HH) appeared at 7.00, 7.03, and 7.05 ppm, respectively.

^{1}HNMR spectrum of $P3HT_{21000}$-*b*-PEG_{750} block copolymers is represented in Fig. 3(a), in which all peaks are identified on the structure of diblock copolymer. In addition, Fig. 3(b) illustrates the size exclusion chromatography (SEC) elutograms

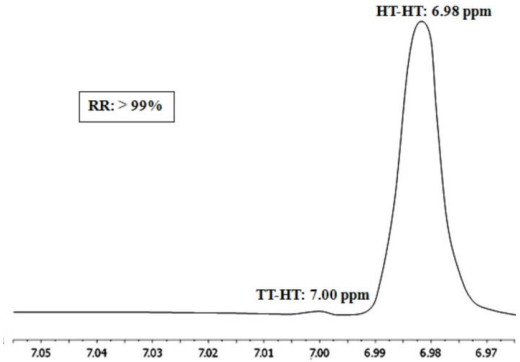

(a)

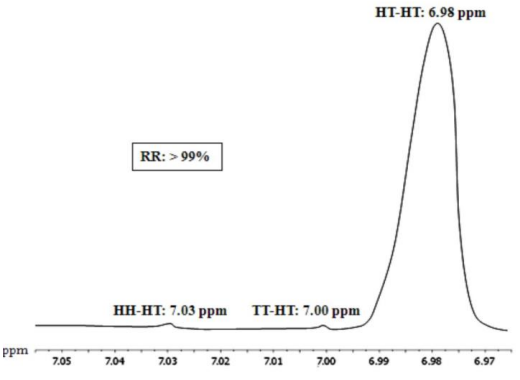

(b)

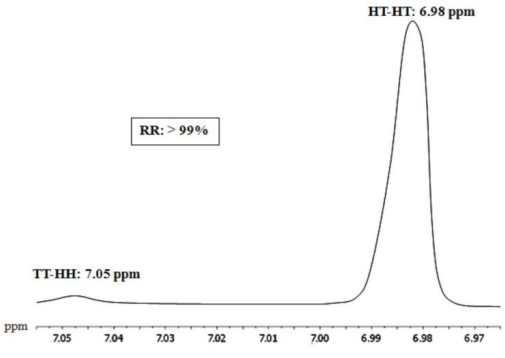

(c)

Fig. 2- 1HNMR spectra of P3HT48800-Br (a), P3HT21000-Br (b), and P3HT7150-Br (c).

of $P3HT_{7000}$-*b*-PEG_{750}, $P3HT_{21000}$-*b*-PEG_{750}, and $P3HT_{48800}$-*b*-PEG_{750} block copolymers. The PDI of synthesized P3HT-*b*-PEG block copolymers ranged in 1.23–1.26.

Fig. 4(a) reports the thermogravimetric analysis (TGA) curves of PEG_{750} (200–398 °C), $P3HT_{21000}$ (> 460 °C)-*b*-PEG_{750} (395–460 °C), and $P3HT_{21000}$ (> 470 °C) homo and block copolymers. The ultraviolet-visible (UV-Vis) spectra of $P3HT_{48800}$-*b*-PEG_{750} in tetrahydrofuran (THF) and anisole are also reported in Fig. 4(b). In a better solvent such as THF, only one main peak was detected at 462 nm. Via using a poorer solvent like anisole, in addition to the red-shifted main peak of 504 nm, two shoulder peaks also appeared at 571 and 602 nm. The two vibronic peaks were attributed to the absorption of strong interchain π-π interactions. The synthesized materials were utilized to develop the fibrillar conductive single crystals in different growth conditions.

By applying the self-seeding technique, a uniform and homogeneous population of conductive P3HT single crystals covered by the dielectric coily PEG brushes were developed. Figs. 5(a-c) depict AFM height image, phase image, and height profile of $P3HT_{7150}$-*b*-PEG single crystals grown from toluene at T_s = 20 °C, T_c = 10 °C. The dimensions of these single crystals in a (thickness of single crystal or hexyl side chains or (100) direction), b (length of single crystal or π-π stacking or (020) direction), and c (width of single crystal or longitude of P3HT main backbones) axes were 103.29 nm, 39.81 μm, and 38.29 nm, respectively. The folding numbers

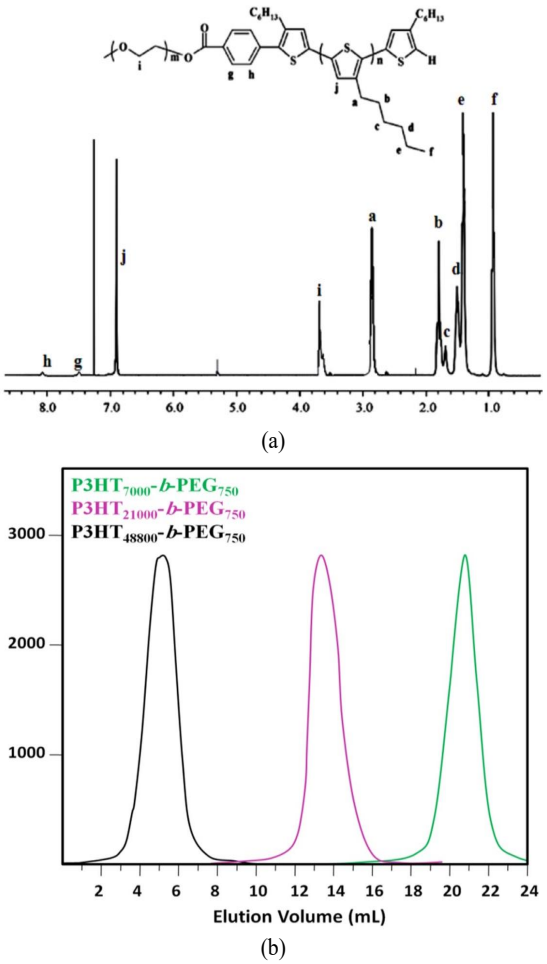

Fig. 3- (a) 1HNMR spectra of synthesized P3HT21000-b-PEG750 block copolymers; (b) SEC elutograms of P3HT7000-b-PEG750, P3HT21000-b-PEG750, and P3HT48800-b-PEG750 block copolymers.

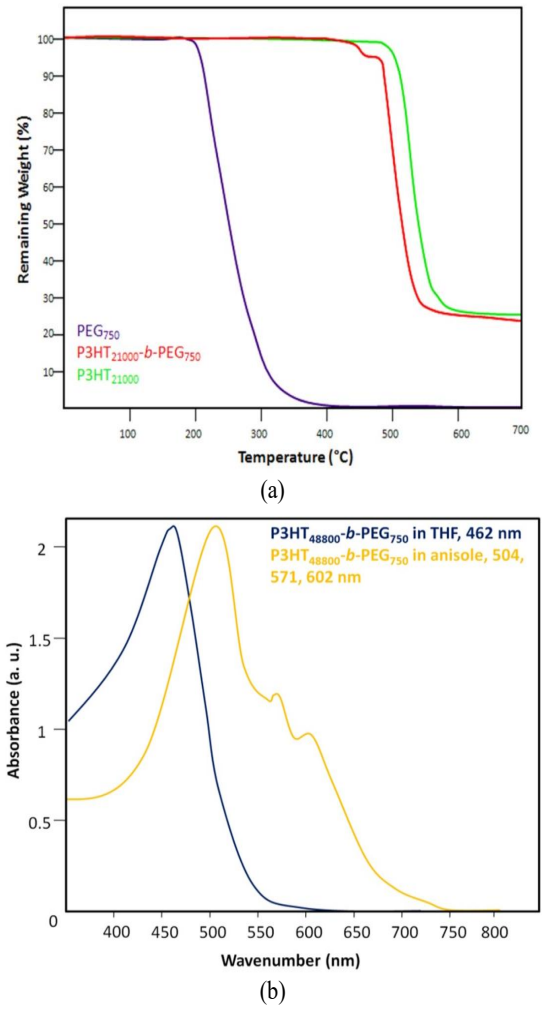

Fig. 4- (a) TGA curves of PEG750 (200–398 °C), P3HT21000 (> 460 °C)-b-PEG750 (395–460 °C), and P3HT21000 (> 470 °C); (b) UV-Vis spectra of P3HT48800-b-PEG750 in THF and anisole.

for homopolymer single crystals were obtained by dividing the P3HT extended length to width of single crystals, i.e., $D_{(002)}$ dimension detected from the width of AFM height profile in the edge-on oriented single crystals and from the height of AFM height profile in the flat-on oriented single crystals. The extended length for molecular weights of 7150, 21000, and 48800 g/mol were 18, 53, and 122 nm, respectively [20]. Indeed, the PEG coily blocks were excluded from the P3HT crystalline structure during growth of single crystals and, consequently, they developed some brush-like or hairy regions. Figs. 6(a) and (b) compare AFM height images and height profiles of $P3HT_{48800}$-*b*-PEG hairy single crystals and $P3HT_{48800}$ non-hairy single crystals grown from anisole at T_s = 60 °C and T_c = 20 °C. In

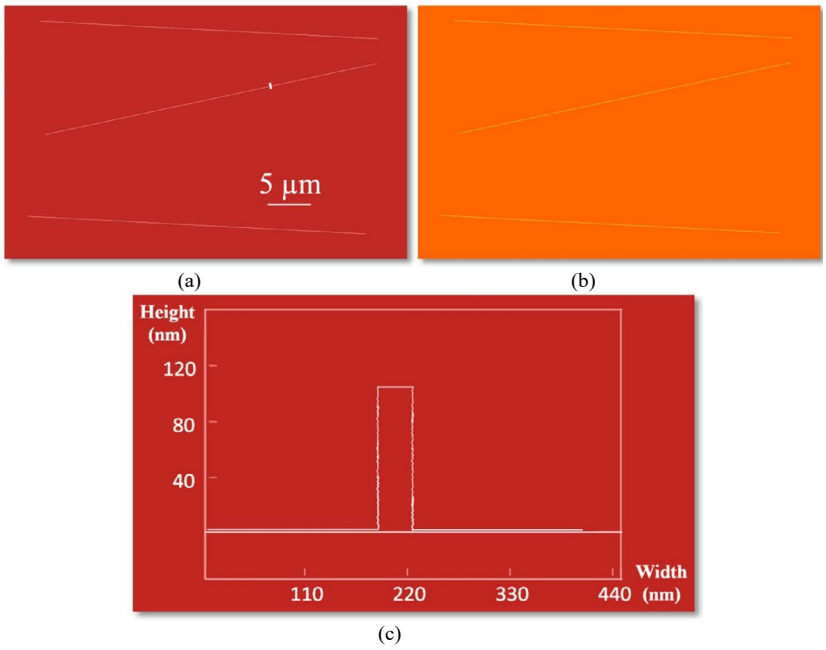

Fig. 5- AFM height image (a), phase image (b) and height profile (c) of P3HT7150-b-PEG single crystals grown from toluene at Ts = 20 °C, Tc = 10 °C.

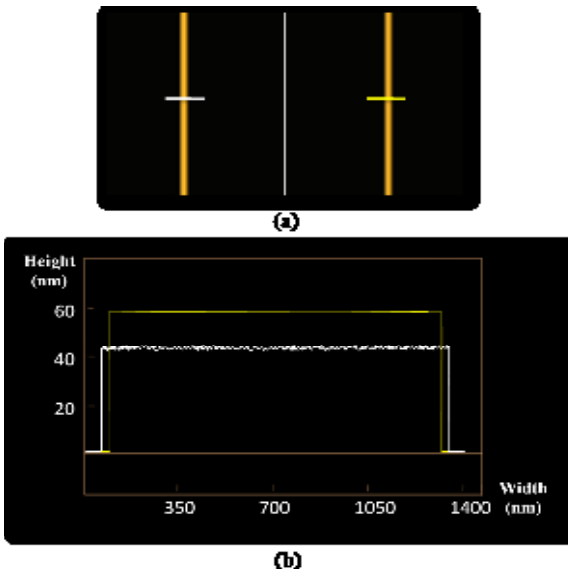

Fig. 6- AFM height images and height profiles of P3HT48800-b-PEG hairy single crystal (white), a = 1313.27 nm, b = 148.10 µm, c = 42.42 nm; and P3HT48800 non-hairy single crystal (yellow), a = 1289.22 nm, b = 143.60 µm, c = 58.50 nm grown from anisole at Ts = 60 °C, Tc = 20 °C.

the flat-on oriented hairy single crystals, the wavy AFM height profile (white curve in Figure 6(b)) demonstrated the accumulation of coily dielectric PEG end blocks on the surface of single crystals in c axis. However, AFM height profile of $P3HT_{48800}$ non-hairy single crystal was straight without any waves (yellow curve in Figure 6(b)). All data in this section are tabulated in Tables S1, S2, and S3.

AFM images accompanied by selected area electron diffraction (SAED) patterns in the inset panels for some P3HT based fibrillar single crystals are represented in Figs. 7(a-e). The dimensions of these single crystals in a (thickness of single crystal or hexyl side chains or (100) direction), b (length

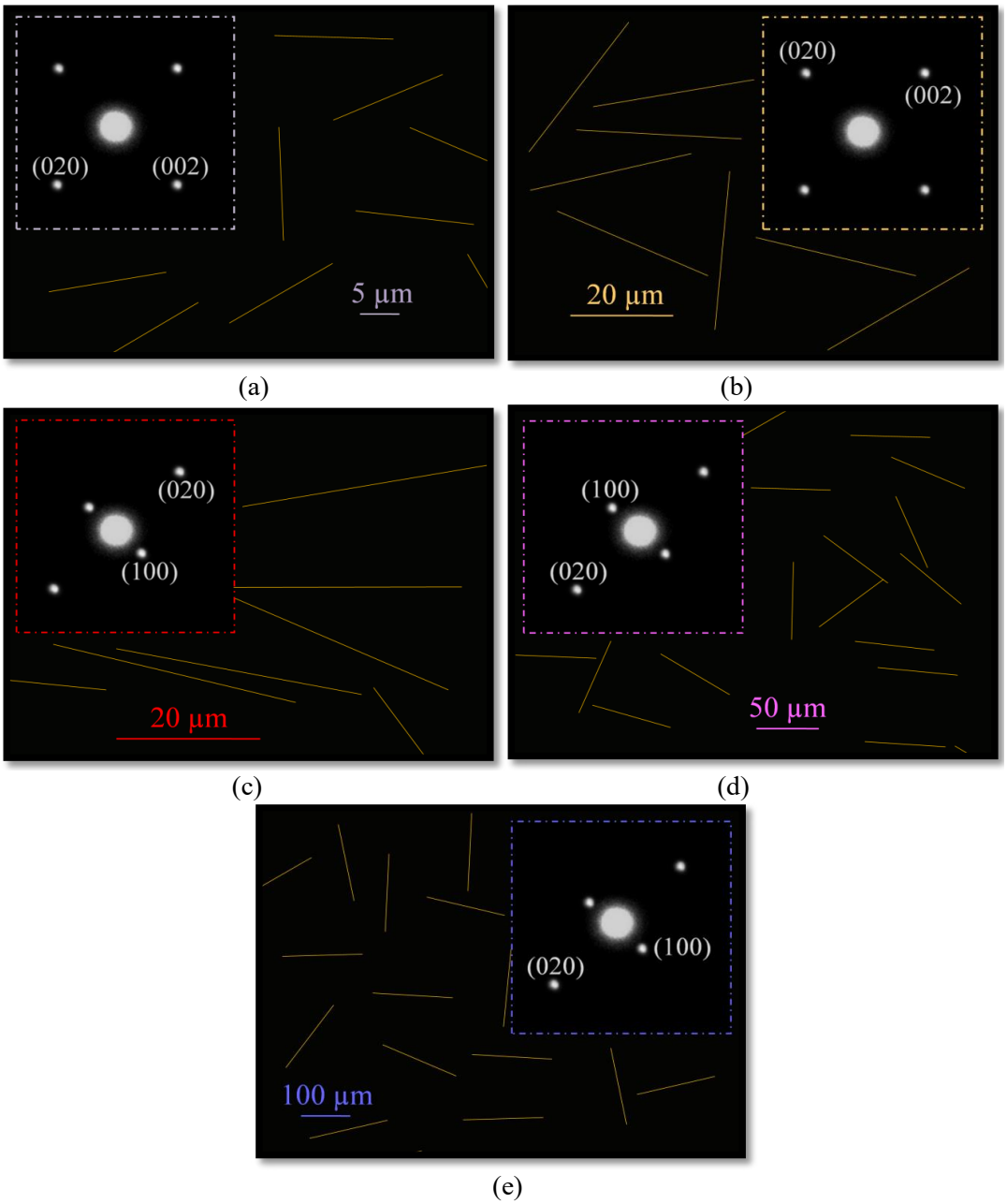

Fig. 7- AFM images of (a) P3HT7150 single crystals in toluene, Ts = 20 °C, Tc = 0 °C, a = 106.12 nm, b = 30.20 µm, c = 137.00 nm; (b) P3HT21000-b-PEG single crystals in toluene, Ts = 20 °C, Tc = 0 °C, a = 101.29 nm, b = 32.15 µm, c = 104.81 nm; (c) P3HT48800 single crystals in toluene, Ts = 30 °C, Tc = 20 °C, a = 74.78 nm, b = 34.74 µm, c = 58.50 nm; (d) P3HT48800 single crystals in xylene, Ts = 40 °C, Tc = 30 °C, a = 437.50 nm, b = 64.55 µm, c = 116.87 nm; (e) P3HT7150-b-PEG single crystals in anisole, Ts = 50 °C, Tc = 40 °C, a = 1089.50 nm, b = 161.88 µm, c = 38.35 nm.

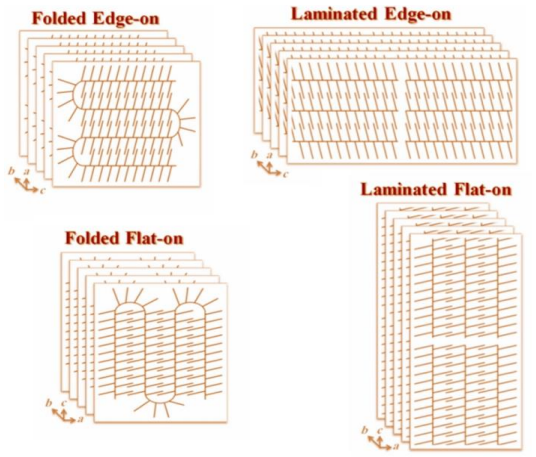

Fig. 8- Scheme of backbone folding in high molecular weight P3HTs in edge-on and flat-on oriented single crystals as well as backbone lamination in low molecular weight P3HTs in edge-on and flat-on oriented single crystals.

of single crystal or π-π stacking or (020) direction), and c (width of single crystal or longitude of P3HT main backbones) axes are also reported in the caption. In SAED pattern of the fibrillar P3HT single crystals having (020) prisms in π-π stacking direction and (002) in longitude of P3HT backbone, an edge-on orientation was recorded, in which the P3HT main backbones and the hexyl side chains were parallel with and perpendicular to the substrate, respectively. On the other hand, appearance of two pairs of (100) prisms in a axis or hexyl side chains direction and two pairs of (020) prisms in b axis or π-π stacking direction demonstrated a flat-on orientation for the P3HT chains, in which the main backbones and hexyl side chains were perpendicular to and parallel with the substrate, respectively. The schemes of Fig. 8 represent the folded edge-on and laminated edge-

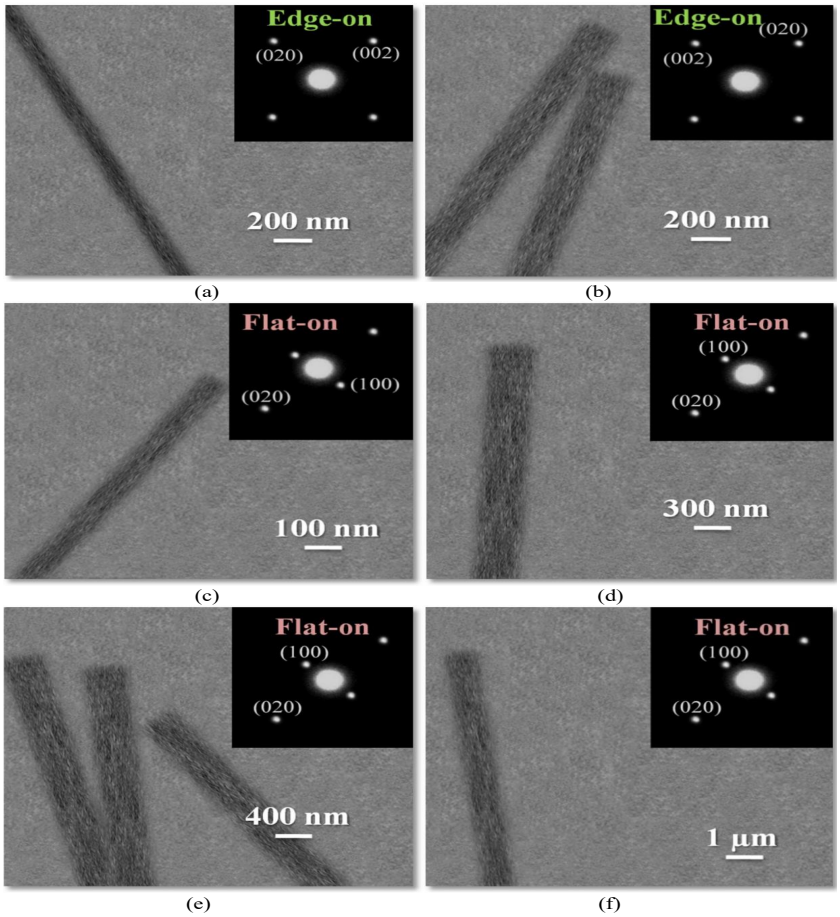

Fig. 9. TEM images accompanied by the corresponding SAED patterns in the inset for (a) P3HT7150 single crystals in toluene, Ts = 30 °C, Tc = 0 °C, a = 130.00 nm, b = 41.00 μm, c = 136.85 nm; (b) P3HT21000 single crystals in toluene, Ts = 30 °C, Tc = 0 °C, a = 108.22 nm, b = 37.00 μm, c = 201.55 nm; (c) P3HT48800-b-PEG single crystals in toluene, Ts = 30 °C, Tc = 10 °C, a = 83.00 nm, b = 36.87 μm, c = 23.04 nm; (d) P3HT48800-b-PEG single crystals in xylene, Ts = 30 °C, Tc = 20 °C, a = 385.59 nm, b = 57.94 μm, c = 32.83 nm; (e) P3HT48800-b-PEG single crystals in xylene, Ts = 40 °C, Tc = 30 °C, a = 445.76 nm, b = 67.53 μm, c = 42.46 nm; (f) P3HT7150 single crystals in anisole, Ts = 50 °C, Tc = 40 °C, a = 1045.02 nm, b = 130.84 μm, c = 821.75 nm.

on P3HT chains for the high molecular weight (48000 g/mol) and low molecular weight (21000 and 7150 g/mol) P3HTs, respectively. Figs. 9(a-f) also report TEM images accompanied by the corresponding SAED patterns in the inset for the P3HT based homopolymer and block copolymer single crystals developed in distinct processing conditions.

The 2D GIWAXS plots of $P3HT_{48800}$-*b*-PEG single crystals grown from xylene at T_s = 30 °C, T_c = 10 °C and grown from anisole at T_s = 50 °C, T_c = 20 °C are represented in Figs. 10(a) and (b), respectively. The edge-on orientation was dominant in this work; because (100) growth planes (hexyl side chains direction) and (020) growth planes (π-π stacking direction) mainly appeared in out of plane (OOP or Q_z) and in plane (IP or Q_{xy}) axes, respectively. In the single crystals grown with an edge-on orientation, the hexyl side chains were perpendicular to substrate. Appearance of (200) and (300) spots in addition to (100) planes in Q_z was indicative of a high ordering in the structures of developed fibrillar $P3HT_{48800}$-*b*-PEG single crystals.

Based on AFM data and the extended length of P3HT backbones, the P3HT chains with lower molecular weights (7150 and 21000 g/mol) depicted backbone laminating states, however, those with M_n^{P3HT} of 48800 g/mol were folded in c direction. The effective factors on folding of $P3HT_{48800}$ chains in the single crystal structures consisted of the quality of employed solvent and the crystallization temperature. Better solvents due to decelerating the growth condition led to a higher number of foldings. The folding numbers for $P3HT_{48800}$-*b*-PEG single crystals grown at T_s = 30 °C and T_c = 20 °C from toluene and xylene were 4 and 3, respectively. Furthermore, the folding number mainly decreased with an increase of T_c. The free energy increases parallel with the crystallization temperature elevation. To reach a lower free energy and, consequently, a stable state, the crystal tends to decrease its folding number. Because the extended chains possess the lowest energy and thus the most stable state. In conclusion, via T_c enhancement, the system would decrease the folding number to maintain its stability [53]. For $P3HT_{48800}$-*b*-PEG single crystals grown from toluene, the folding numbers at T_c = 0 and 10 °C were 5, and via T_c elevation to 20 °C, this value decreased to 4. Moreover, for $P3HT_{48800}$-*b*-PEG single crystals grown from anisole at T_s = 60 °C, the folding numbers at the crystallization temperatures of 20, 30, and 40 °C were 1, 1, and 0, respectively. In $P3HT_{7150}$-*b*-PEG and $P3HT_{21000}$-*b*-PEG single crystals, due to the presence of end coily PEG blocks, only two backbone lamination was allowed in c direction.

Towards an optimum seeding temperature, the remained seeds were larger but in a lower population. Hence, in secondary growth step, larger seeds resulted in bigger single crystals. This trend was detected for toluene, xylene, and anisole. In toluene, the dimension of single crystals in a direction (thickness or $D_{(100)OOP}$) at T_c = 10 °C for $P3HT_{7150}$-*b*-PEG single crystals at T_s = 20 °C was 103.29 nm and at T_s = 30 °C was 130.17 nm, respectively. In xylene, the thickness of single crystals at T_c = 20 °C for $P3HT_{21000}$-*b*-PEG single

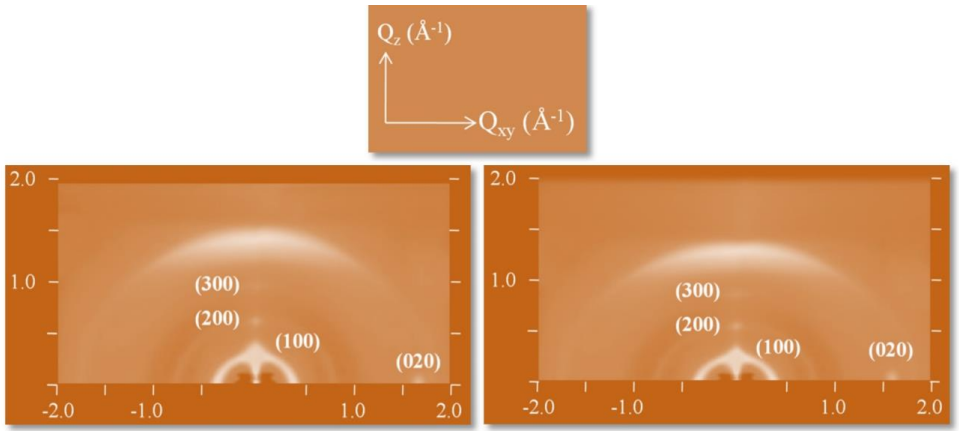

Fig. 10. 2D GIWAXS plots of P3HT48800-b-PEG single crystals grown from xylene at Ts = 30 °C, Tc = 10 °C (a) as well as grown from anisole at Ts = 50 °C, Tc = 20 °C (b).

crystals at T_s = 30 °C was 437.01 nm and at T_s = 40 °C was 555.17 nm, respectively. In anisole, the thickness of single crystals at T_c = 40 °C for $P3HT_{48800}$-*b*-PEG single crystals at T_s = 50 °C was 1001.13 nm and at T_s = 60 °C was 1172.16 nm, respectively.

As a fact, the growth of single crystal encountered a higher hindrance in a direction by increasing the molecular weight of P3HT backbones. In xylene at T_s = 40 °C and T_c = 10 °C, $D_{(100)OOP}$ for $P3HT_{7150}$-*b*-PEG single crystals was 638.10 nm, for $P3HT_{21000}$-*b*-PEG single crystals was 606.43 nm, and for $P3HT_{48800}$-*b*-PEG single crystals was 555.28 nm. This trend was also detected in two other solvents, i.e., toluene and anisole. In our growth systems, poorer solvents led to thicker single crystals. At T_s = 30 °C and T_c = 20 °C, the thickness of $P3HT_{48800}$-*b*-PEG single crystals in toluene was 77.03 nm and in xylene was and 385.59 nm. By increasing the crystallization temperature, $D_{(100)OOP}$ values decreased; because a higher T_c provided a lower driving force for stacking the P3HT chains in an or hexyl chains direction. In toluene, $D_{(100)OOP}$ at T_s = 30 °C for $P3HT_{21000}$-*b*-PEG single crystals at T_c = 0 °C was 115.08 nm and at T_c = 20 °C was 98.00 nm. Moreover, in xylene at T_s = 40 °C, $D_{(100)OOP}$ for $P3HT_{48800}$-*b*-PEG single crystals grown at T_c = 10 °C was 555.28 nm, and grown at T_c = 30 °C was 445.76 nm, respectively. All data in this section are tabulated in Tables S1, S2, and S3.

Similar to the effect of solvent quality on the

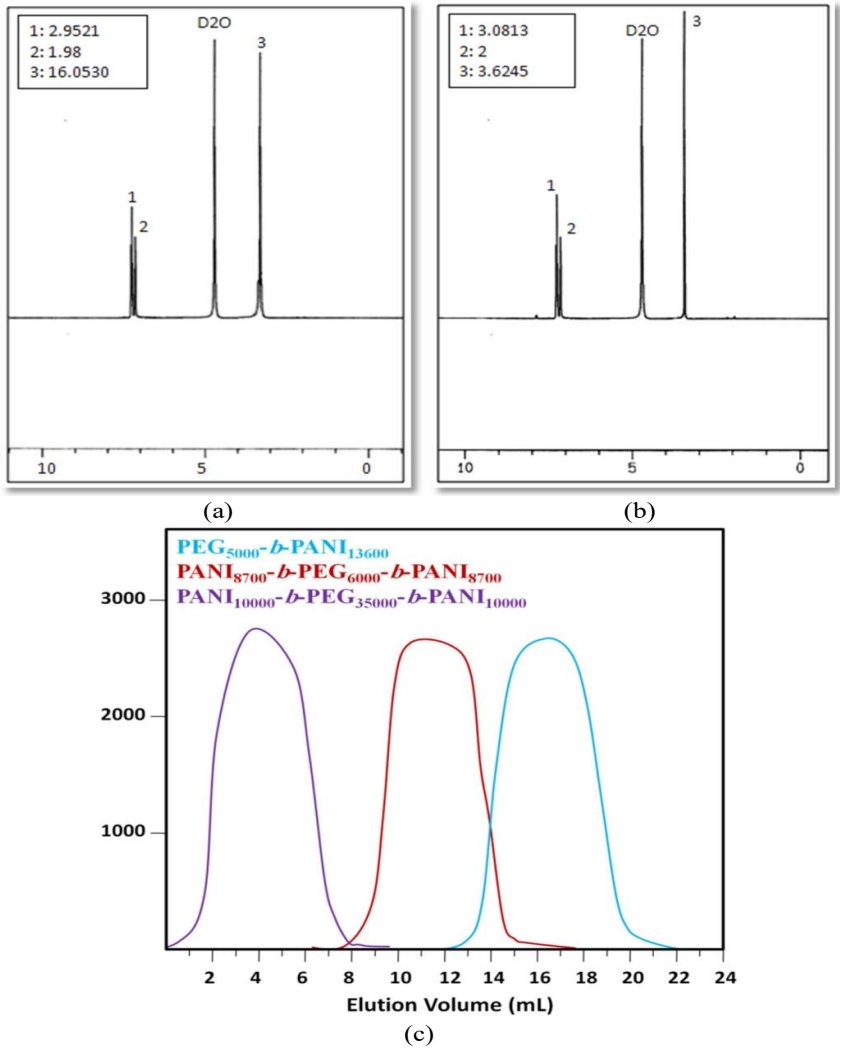

Fig. 11. 1HNMR spectra of PEG5000-b-PANI3100 (a) and PANI8700-b-PEG6000-b-PANI8700 (b); SEC elutograms of PEG5000-b-PANI13600, PANI8700-b-PEG6000-b-PANI8700, and PANI10000-b-PEG35000-b-PANI10000 block copolymers (c).

thickness or hexyl side chains stacking, poorer solvents also resulted in further stacking in π-π stacking. At T_s = 30 °C and T_c = 20 °C, the length of fibrillar P3HT$_{48800}$-*b*-PEG single crystals or $D_{(020)IP}$ value in toluene was 36.78 μm and in xylene was 57.94 μm. Besides, at T_s = 30 °C and T_c = 10 °C, the length of fibrillar P3HT$_{7150}$-*b*-PEG single crystals in toluene was 49.75 μm and in xylene was 80.38 μm. At higher seeding temperatures, larger seeds remained, thereby grown single crystals were longer in π-π stacking direction. Quantitatively, $D_{(020)IP}$ values for P3HT$_{21000}$-*b*-PEG single crystals grown from toluene at seeding temperatures of 20 and 30 °C were 32.15 and 41.10 μm (at T_c = 0 °C), grown from xylene at seeding temperatures of 30 and 40 °C were 67.98 and 81.79 μm (at T_c = 20 °C), and grown from anisole at seeding temperatures of 50 and 60 °C were 143.77 and 162.92 μm (at T_c = 40 °C), respectively. Furthermore, the hindrance against the attachment of longer P3HT backbones to the P3HT crystalline structures was larger, thereby higher molecular weights of P3HT chains led to shorter fibrillar single crystals. This molecular weight effect on the length of grown single crystals was detected for toluene, xylene, and anisole at all processing temperatures. The $D_{(020)IP}$ in toluene at T_s = 20 °C and T_c = 0 °C for P3HT$_{7150}$-*b*-PEG single crystals was 39.96 μm, for P3HT$_{21000}$-*b*-PEG single crystals was 32.15 μm, and for P3HT$_{48800}$-*b*-PEG single crystals was 26.20 μm. Likewise, in xylene at T_s = 40 °C and T_c = 30 °C, $D_{(020)IP}$ for P3HT$_{7150}$-*b*-PEG single crystals was 94.75 μm, for P3HT$_{21000}$-*b*-PEG single crystals was 81.56 μm, and finally for P3HT$_{48800}$-*b*-PEG single crystals was 67.53 μm. Furthermore, in anisole at T_s = 60 °C and T_c = 30 °C, $D_{(020)IP}$ for P3HT$_{7150}$-*b*-PEG single crystals was 180.71 μm, for P3HT$_{21000}$-*b*-PEG single crystals was 163.00 μm, and finally for P3HT$_{48800}$-*b*-PEG single crystals was 147.75 μm.

In upcoming section, the role of PEG blocks was altered from coily brushes to crystalline substrates using PEG$_{5000}$-*b*-PANI, PANI-*b*-PEG$_{6000}$-*b*-PANI, and PANI-*b*-PEG$_{35000}$-*b*-PANI block copolymers instead of P3HT-*b*-PEG ones. Via changing the crystalline building blocks from P3HT to PEG, the rectangular crystals were developed instead of fibrillar ones.

3.2. Square PEG single crystals sandwiched between PANI nanorods

^{1}HNMR spectra of PEG$_{5000}$-*b*-PANI$_{3100}$ and PANI$_{8700}$-*b*-PEG$_{6000}$-*b*-PANI$_{8700}$ block copolymers

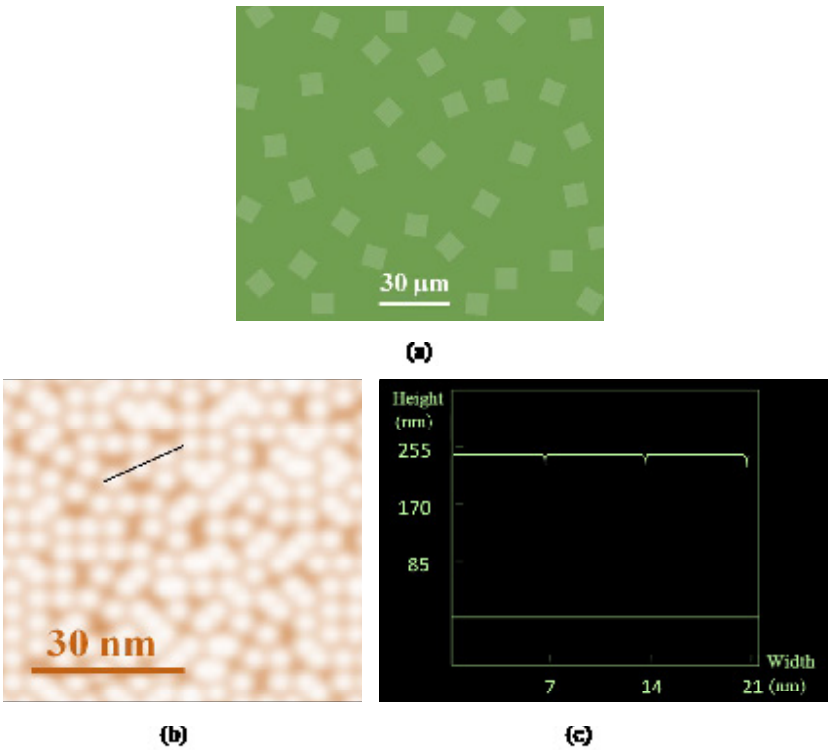

Fig. 12- STEM image of PEG5000-b-PANI3100 single crystals grown from amyl acetate at Tc = 23 °C (a); AFM height image (b) and height profile (c) of PEG5000-b-PANI13600 single crystals grown from amyl acetate at Tc = 28 °C.

are represented in Figs. 11(a) and (b), respectively. The molecular weights of block copolymers were calculated based on the integral ratios of protons of PANI benzene ring (7.2–7.4 ppm) and CH_2 protons of PEG (3.5 ppm). Moreover, Fig. 11(c) demonstrates the SEC traces of PEG_{5000}-*b*-$PANI_{13600}$, $PANI_{8700}$-*b*-PEG_{6000}-*b*-$PANI_{8700}$, and $PANI_{10000}$-*b*-PEG_{35000}-*b*-$PANI_{10000}$ block copolymers. The PDI of synthesized PEG-*b*-PANI block copolymers ranged in 1.62–1.68.

The self-seeding technique was also employed to develop PEG single crystals covered by the PANI nanorods. In these types of single crystals, the dielectric coily PEG chains assembled as the folded crystalline substrates, and the PANI rigid blocks excluded from the crystalline structures arranged as the rod nano-brushes on PEG substrates. In PANI-*b*-PEG_{35000}-*b*-PANI single crystals via elevation of T_c, the thickness of substrate increased and, consequently, the folding number decreased. So, the required surface area of lower diameters was provided. The approximate folding number for the lamellar PEG substrate was determined based on extended length of PEG chains and crystalline substrate thickness acquired from SAXS measurements [58]. In PANI-*b*-PEG_{6000}-*b*-PANI and PEG_{5000}-*b*-PANI single crystals, the thickness of substrate did not vary by increase of PANI molecular weight. This was due to the extended conformation of PANI brushes on the PEG_{5000} and PEG_{6000} substrates. Through lengthening the PANI nanofibers, their exerted osmotic pressure onto substrate surface did not change. Fig. 12(a) illustrates the scanning transmission electron microscopy (STEM) image of PEG_{5000}-*b*-$PANI_{3100}$ single crystals grown from amyl acetate at T_c = 23 °C. The oxidant used to prepare PEG_{5000}-*b*-$PANI_{3100}$ block copolymers was PHD. It could be inferred that all single crystals were uniform from the perspective of lateral size and shape. AFM height image and height profile of PEG_{5000}-*b*-$PANI_{13600}$ single crystals grown from amyl acetate at T_c = 28 °C are also depicted in Figs. 12(b) and (c), respectively. The oxidant used to prepare PEG_{5000}-*b*-$PANI_{13600}$ block copolymers was PHD. In these single crystals, the thickness of crystalline PEG substrate, the height of stretched PANI nanorods, and their average diameter were 2.81, 121, and 6 nm, respectively.

With increasing the molecular weight of PANI nanorods, the height of PANI nano-brushes increased on PEG single crystals. This trend stood for all samples at whole temperature ranges. By increasing the PANI repeating units from 34 to 95 and to 154 with the oxidant of APS, the thicknesses of PANI nanorods were 28, 83, and 127 nm, respectively. At the same crystallization temperature with PHD oxidant and repeating units of 38, 98, and 158, the heights of PANI nanorods were 33, 80, and 133 nm, respectively. Neither PEG_{5000}-*b*-PANI nor PANI-*b*-PEG_{6000}-*b*-PANI single crystals having

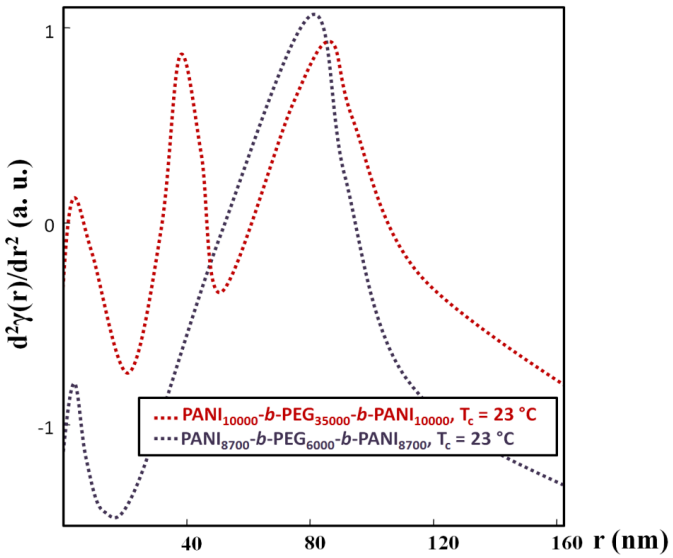

Fig. 13. 1D SAXS graphs of PANI10000-b-PEG35000-b-PANI10000 and PANI8700-b-PEG6000-b-PANI8700 single crystals grown from amyl acetate at Tc = 23 °C.

various PANI molecular weights grew above 28 °C. Because above 28 °C due to enhancement of PEG substrate thickness and, consequently, foldings decrease, the demanded surface area of PANI nanorods with a minimum diameter of 6 nm for PEG_{5000} systems and 6–7 nm for PEG_{6000} ones were not provided anymore by PEG substrate. All data in this section are tabulated in Tables S4, S5, and S6.

In PEG_{5000}-*b*-PANI and PANI-*b*-PEG_{6000}-*b*-PANI single crystals, the interface distribution function (IDF) of SAXS graphs depicted only two different peaks. The first and second peaks stood for the PEG crystalline substrate thickness and the height of grafted PANI nanorods on the substrate surface. In IDF of SAXS for PANI-*b*-PEG_{35000}-*b*-PANI single crystals, the first peak was for the thickness of crystalline substrate, and second and third peaks indicated the thickness of PANI nanorods in the non-stretched and stretched phase regions, respectively. The 1D SAXS graphs of $PANI_{10000}$-*b*-PEG_{35000}-*b*-$PANI_{10000}$ (3.80, 38.00, and 86.01 nm) and $PANI_{8700}$-*b*-PEG_{6000}-*b*-$PANI_{8700}$ (3.24 and 81.00 nm) single crystals grown from amyl acetate at T_c = 23 °C are represented in Fig. 13. The oxidant used to prepare $PANI_{10000}$-*b*-PEG_{35000}-*b*-$PANI_{10000}$ and $PANI_{8700}$-*b*-PEG_{6000}-*b*-$PANI_{8700}$ block copolymers was APS.

4. Conclusions

The conductive P3HT single crystals covered by the dielectric coily PEG oligomers were grown from toluene, xylene, and anisole. Longer P3HT backbones resulted in folding, whereas shorter ones were laminated on each other. The solvent quality and crystallization temperature affected the chain folding in the fibrillar P3HT single crystals. Thanks to a lower crystallization rate in good solvents, a large number of foldings were detected in the longitude of main backbones. The poorer solvents increased the dimensions of grown crystals in both hexyl side chains and π-π stacking directions. The crystallization temperature had an inverse impact on the folding number in order to resume the system stability. In the second empirical part, to change the role of PEG blocks from random coily brushes to the single crystalline substrates, PANI-*b*-PEG-*b*-PANI rod-coil block copolymers were applied and the conductive PANI nanorods were developed on PEG lamellar single crystals. The molecular weights of PANI and PEG blocks as well as crystallization temperature were investigated as effective parameters on the system characteristics.

References:

1. Lu L, Zheng T, Wu Q, Schneider AM, Zhao D, Yu L. Recent Advances in Bulk Heterojunction Polymer Solar Cells. Chemical Reviews. 2015;115(23):12666-731.
2. Kim JS, Lee JH, Park JH, Shim C, Sim M, Cho K. High-Efficiency Organic Solar Cells Based on Preformed Poly(3-hexylthiophene) Nanowires. Advanced Functional Materials. 2010;21(3):480-6.
3. Kim J-H, Park JH, Lee JH, Kim JS, Sim M, Shim C, et al. Bulk heterojunction solar cells based on preformed polythiophene nanowires via solubility-induced crystallization. Journal of Materials Chemistry. 2010;20(35):7398.
4. Kim M, Jo SB, Park JH, Cho K. Flexible lateral organic solar cells with core–shell structured organic nanofibers. Nano Energy. 2015;18:97-108.
5. Liu F, Chen D, Wang C, Luo K, Gu W, Briseno AL, et al. Molecular Weight Dependence of the Morphology in P3HT:PCBM Solar Cells. ACS Applied Materials & Interfaces. 2014;6(22):19876-87.
6. Bruner C, Novoa F, Dupont S, Dauskardt R. Decohesion Kinetics in Polymer Organic Solar Cells. ACS Applied Materials & Interfaces. 2014;6(23):21474-83.
7. Agbolaghi S, Abbasi F, Gheybi H. High efficient and stabilized photovoltaics via morphology manipulating in active layer by rod-coil block copolymers comprising different hydrophilic to hydrophobic dielectric blocks. European Polymer Journal. 2016;84:465-80.
8. Agbolaghi S, Nazari M, Zenoozi S, Abbasi F. The highest power conversion efficiencies in poly(3-hexylthiophene)/fullerene photovoltaic cells modified by rod-coil block copolymers under different annealing conditions. Journal of Materials Science: Materials in Electronics. 2017;28(14):10611-24.
9. Agbolaghi S, Abbasi F, Zenoozi S, Nazari M. Annealing-free multi-thermal techniques comprising aging, cycling and seeding to enhance performance of thick P3HT:PCBM photovoltaic cells via developing hairy crystals. Materials Science in Semiconductor Processing. 2017;63:285-94.
10. Zenoozi S, Agbolaghi S, Poormahdi E, Hashemzadeh-Gargari M, Mahmoudi M. Verification of Scherrer formula for well-shaped poly(3-hexylthiophene)-based conductive single crystals and nanofibers and fabrication of photovoltaic devices from thin film coating. Macromolecular Research. 2017;25(8):826-40.
11. Agbolaghi S, Ebrahimi S, Massoumi B, Abbaspoor S, Sarvari R, Abbasi F. Enhanced properties of photovoltaic devices tailored with novel supramolecular structures based on reduced graphene oxide nanosheets grafted/functionalized with thiophenic materials. Journal of Polymer Science Part B: Polymer Physics. 2017;55(24):1877-89.
12. Bao Z, Dodabalapur A, Lovinger AJ. Soluble and processable regioregular poly(3-hexylthiophene) for thin film field-effect transistor applications with high mobility. Applied Physics Letters. 1996;69(26):4108-10.
13. Yu X, Xiao K, Chen J, Lavrik NV, Hong K, Sumpter BG, et al. High-Performance Field-Effect Transistors Based on Polystyrene-b-Poly(3-hexylthiophene) Diblock Copolymers. ACS Nano. 2011;5(5):3559-67.
14. Liu H, Reccius CH, Craighead HG. Single electrospun regioregular poly(3-hexylthiophene) nanofiber field-effect transistor. Applied Physics Letters. 2005;87(25):253106.
15. Lee J-Y, Lin C-J, Lo C-T, Tsai J-C, Chen W-C. Synthesis, Morphology, and Field-Effect Transistor Characteristics of Crystalline Diblock Copolymers Consisted of Poly(3-hexylthiophene) and Syndiotactic Polypropylene. Macromolecules. 2013;46(8):3005-14.
16. Lim JA, Kim J-H, Qiu L, Lee WH, Lee HS, Kwak D, et al.

Inkjet-Printed Single-Droplet Organic Transistors Based on Semiconductor Nanowires Embedded in Insulating Polymers. Advanced Functional Materials. 2010;20(19):3292-7.
17. Burroughes JH, Bradley DDC, Brown AR, Marks RN, Mackay K, Friend RH, et al. Light-emitting diodes based on conjugated polymers. Nature. 1990;347(6293):539-41.
18. Thomas SW, Joly GD, Swager TM. Chemical Sensors Based on Amplifying Fluorescent Conjugated Polymers. Chemical Reviews. 2007;107(4):1339-86.
19. Qiu L, Lee WH, Wang X, Kim JS, Lim JA, Kwak D, et al. Organic Thin-film Transistors Based on Polythiophene Nanowires Embedded in Insulating Polymer. Advanced Materials. 2009;21(13):1349-53.
20. Rahimi K, Botiz I, Stingelin N, Kayunkid N, Sommer M, Koch FPV, et al. Controllable Processes for Generating Large Single Crystals of Poly(3-hexylthiophene). Angewandte Chemie International Edition. 2012;51(44):11131-5.
21. Hourani W, Rahimi K, Botiz I, Vinzenz Koch FP, Reiter G, Lienerth P, et al. Anisotropic charge transport in large single crystals of π-conjugated organic molecules. Nanoscale. 2014;6(9):4774.
22. Dong H, Jiang S, Jiang L, Liu Y, Li H, Hu W, et al. Nanowire Crystals of a Rigid Rod Conjugated Polymer. Journal of the American Chemical Society. 2009;131(47):17315-20.
23. Goto H, Okamoto Y, Yashima E. Solvent-Induced Chiroptical Changes in Supramolecular Assemblies of an Optically Active, Regioregular Polythiophene. Macromolecules. 2002;35(12):4590-601.
24. Kim DH, Han JT, Park YD, Jang Y, Cho JH, Hwang M, et al. Single-Crystal Polythiophene Microwires Grown by Self-Assembly. Advanced Materials. 2006;18(6):719-23.
25. Ma Z, Geng Y, Yan D. Extended-chain lamellar packing of poly(3-butylthiophene) in single crystals. Polymer. 2007;48(1):31-4.
26. Kim DH, Park YD, Jang Y, Yang H, Kim YH, Han JI, et al. Enhancement of Field-Effect Mobility Due to Surface-Mediated Molecular Ordering in Regioregular Polythiophene Thin Film Transistors. Advanced Functional Materials. 2005;15(1):77-82.
27. Kim DH, Park YD, Jang Y, Kim S, Cho K. Solvent Vapor-Induced Nanowire Formation in Poly(3-hexylthiophene) Thin Films. Macromolecular Rapid Communications. 2005;26(10):834-9.
28. Kovacs AJ, Gonthier A. Crystallization and fusion of self-seeded polymers. Aktuelle Probleme der Polymer-Physik III: Steinkopff; 1972. p. 24-.
29. Massa MV, Lee MSM, Dalnoki-Veress K. Crystal nucleation of polymers confined to droplets: Memory effects. Journal of Polymer Science Part B: Polymer Physics. 2005;43(23):3438-43.
30. Maus A, Hempel E, Thurn-Albrecht T, Saalwächter K. Memory effect in isothermal crystallization of syndiotactic polypropylene --Role of melt structure and dynamics? The European Physical Journal E. 2007;23(1):91-101.
31. Agbolaghi S, Zenoozi S, Hosseini Z, Abbasi F. Scrolled/Flat Crystalline Structures of Poly(3-hexylthiophene) and Poly(ethylene glycol) Block Copolymers Subsuming Unseeded Half-Ring-Like and Seeded Cubic, Epitaxial, and Fibrillar Crystals. Macromolecules. 2016;49(24):9531-41.
32. Zenoozi S, Agbolaghi S, Nazari M, Abbasi F. Thermal and optical properties of nano/micro single crystals and nanofibers obtained from semiconductive-dielectric poly(3-hexylthiophene) block copolymers. Materials Science in Semiconductor Processing. 2017;64:85-94.
33. Xiao X, Hu Z, Wang Z, He T. Study on the Single Crystals of Poly(3-octylthiophene) Induced by Solvent-Vapor Annealing. The Journal of Physical Chemistry B. 2009;113(44):14604-10.
34. Xiao X, Wang Z, Hu Z, He T. Single Crystals of Polythiophene with Different Molecular Conformations Obtained by Tetrahydrofuran Vapor Annealing and Controlling Solvent Evaporation. The Journal of Physical Chemistry B. 2010;114(22):7452-60.
35. Rahimi K, Botiz I, Agumba JO, Motamen S, Stingelin N, Reiter G. Light absorption of poly(3-hexylthiophene) single crystals. RSC Adv. 2014;4(22):11121-3.
36. Ihn KJ, Moulton J, Smith P. Whiskers of poly(3-alkylthiophene)s. Journal of Polymer Science Part B: Polymer Physics. 1993;31(6):735-42.
37. Liu J, Sun Y, Gao X, Xing R, Zheng L, Wu S, et al. Oriented Poly(3-hexylthiophene) Nanofibril with the π–π Stacking Growth Direction by Solvent Directional Evaporation. Langmuir. 2011;27(7):4212-9.
38. Oh JY, Shin M, Lee TI, Jang WS, Min Y, Myoung J-M, et al. Self-Seeded Growth of Poly(3-hexylthiophene) (P3HT) Nanofibrils by a Cycle of Cooling and Heating in Solutions. Macromolecules. 2012;45(18):7504-13.
39. Yu Z, Yan H, Lu K, Zhang Y, Wei Z. Self-assembly of two-dimensional nanostructures of linear regioregular poly(3-hexylthiophene). RSC Adv. 2012;2(1):338-43.
40. Pramanik S, Karak N, Banerjee S, Kumar A. Effects of solvent interactions on the structure and properties of prepared PAni nanofibers. Journal of Applied Polymer Science. 2012;126(3):830-6.
41. Sapurina I, Osadchev AY, Volchek BZ, Trchová M, Riede A, Stejskal J. In-situ polymerized polyaniline films. Synthetic Metals. 2002;129(1):29-37.
42. Wang J, Torardi CC, Duch MW. Polyaniline-related ion-barrier anticorrosion coatings. Synthetic Metals. 2007;157(21):851-8.
43. Wang CY, Mottaghitalab V, Too CO, Spinks GM, Wallace GG. Polyaniline and polyaniline–carbon nanotube composite fibres as battery materials in ionic liquid electrolyte. Journal of Power Sources. 2007;163(2):1105-9.
44. Li X-G, Feng H, Huang M-R, Gu G-L, Moloney MG. Ultrasensitive Pb(II) Potentiometric Sensor Based on Copolyaniline Nanoparticles in a Plasticizer-Free Membrane with a Long Lifetime. Analytical Chemistry. 2011;84(1):134-40.
45. Huang J, Virji S, Weiller BH, Kaner RB. Nanostructured Polyaniline Sensors. Chemistry - A European Journal. 2004;10(6):1314-9.
46. Huang J. Syntheses and applications of conducting polymer polyaniline nanofibers. Pure and Applied Chemistry. 2006;78(1).
47. Joo J, Epstein AJ. Electromagnetic radiation shielding by intrinsically conducting polymers. Applied Physics Letters. 1994;65(18):2278-80.
48. Guan H, Fan L-Z, Zhang H, Qu X. Polyaniline nanofibers obtained by interfacial polymerization for high-rate supercapacitors. Electrochimica Acta. 2010;56(2):964-8.
49. Xu H, Li X, Wang G. Polyaniline nanofibers with a high specific surface area and an improved pore structure for supercapacitors. Journal of Power Sources. 2015;294:16-21.
50. Liu S, Wang L, Luo Y, Tian J, Li H, Sun X. Polyaniline nanofibres for fluorescent nucleic acid detection. Nanoscale. 2011;3(3):967.
51. Agbolaghi S, Nazari M, Abbaspoor S, Gheybi H, Abbasi F. Micro/nano conductive-dielectric channels designed by poly(ethylene glycol) single crystals covered by polyaniline nanofibers. Polymer. 2016;92:264-72.
52. Agbolaghi S, Nazari M, Abbaspoor S, Gheybi H, Abbasi F. Characterization of novel extremely extended regime in conductive rod-like polyaniline nanobrush-covered poly(ethylene glycol) single crystals. European Polymer Journal. 2016;82:196-

207.
53. Abbaspoor S, Abbasi F, Agbolaghi S. A novel approach to prepare polymer mixed-brushes via single crystal surface patterning. RSC Adv. 2014;4(33):17071-82.
54. Agbolaghi S, Alizadeh-Osgouei M, Abbaspoor S, Abbasi F. Self-assembling nano mixed-brushes having co-continuous surface morphology by melt growing single crystals and comparison with solution patterned leopard-skin surface morphology. RSC Advances. 2015;5(2):1538-48.
55. Nazari M, Agbolaghi S, Abbaspoor S, Gheybi H, Abbasi F. Arrangement of Conductive Rod Nanobrushes via Conductive–Dielectric–Conductive Sandwiched Single Crystals of Poly(ethylene glycol) and Polyaniline Block Copolymers. Macromolecules. 2015;48(24):8947-57.
56. Agbolaghi S, Abbasi F, Abbaspoor S, Alizadeh-Osgouei M. Self-designed surfaces via single-co-crystallization of homopolymer and diblock copolymers in various growth conditions. European Polymer Journal. 2015;66:108-18.
57. Agbolaghi S, Abbasi F, Abbaspoor S. Epitaxial single crystal surface patterning and study of physical and chemical environmental effects on crystal growth. Colloid and Polymer Science. 2014;292(6):1375-83.
58. Alizadeh-Osgouei M, Agbolaghi S, Abbaspoor S, Abbasi F. A subtle insight into nano-convergence of substrate thickness in melt-grown single-co-crystals. Colloid and Polymer Science. 2016;294(5):869-78.
59. Agbolaghi S, Abbasi F, Abbaspoor S. Preparation of polymer brushes via growth of single crystals of poly(ethylene glycol)-block-polystyrene diblock copolymers synthesized by ATRP and studying the crystal lateral size and brush tethering density. Polymer Bulletin. 2014;71(12):3177-96.
60. Abbaspoor S, Abbasi F, Agbolaghi S. Effects of various polymer brushes on the crystallization of poly(ethylene glycol) in poly(ethylene glycol)-b-polystyrene and poly(ethylene glycol)-b-poly(methyl methacrylate) single crystals. Journal of Polymer Research. 2014;21(8).
61. Abbaspoor S, Agbolaghi S, Abbasi F. Development of nano-channel single crystals and verification of their structures by small angle X-ray scattering. Polymer Bulletin. 2016;74(4):1103-19.
62. Agbolaghi S, Abbasi F, Jalili K. Nascent lateral habits of solution crystallization of poly(ethylene glycol)-block-polystyrene diblock copolymers. Journal of Polymer Research. 2014;21(4).
63. : American Chemical Society (ACS).
64. Lohwasser RH, Thelakkat M. Toward Perfect Control of End Groups and Polydispersity in Poly(3-hexylthiophene) via Catalyst Transfer Polymerization. Macromolecules. 2011;44(9):3388-97.
65. Li F, Shi Y, Yuan K, Chen Y. Fine dispersion and self-assembly of ZnO nanoparticles driven by P3HT-b-PEO diblocks for improvement of hybrid solar cells performance. New J Chem. 2013;37(1):195-203.
66. Kim JY, Frisbie CD. Correlation of Phase Behavior and Charge Transport in Conjugated Polymer/Fullerene Blends. The Journal of Physical Chemistry C. 2008;112(45):17726-36.